Silicon (2022) 14:3091–3100
https://doi.org/10.1007/s12633-021-01080-w

ORIGINAL PAPER

Spectroscopic and Attenuation Shielding Studies on B_2O_3-SiO_2-LiF-ZnO-TiO_2 Glasses

Kh. S. Shaaban [1] · Imed Boukhris [2,3] · Imen Kebaili [2,4] · M. S. Al-Buriahi [5]

Received: 24 January 2021 / Accepted: 22 March 2021 / Published online: 10 April 2021

Abstract

Effects of TiO_2 addition on the spectroscopic and nuclear shielding properties of lithium fluoride zinc titanate borosilicate glasses with the form $59B_2O_3$-$29SiO_2$-2LiF-$(10-x)$ZnO-$xTiO_2$ $x = 0$, 2, 4, 6, 8, *and* 10 mol % labelled as G1-G6, respectively were investigated. The amorphous state of this system was experimentally evaluated using X-ray diffraction. The spectroscopic properties of the recent glasses positively correlated to the increase in TiO_2 content. Molar Refractivity (R_m), molar Polarizability ($\propto_m$),reflection loss (R_L), metallization criterion (M), electron Polarizability ($\alpha°$), ionic concentration (Ni), titanium-titanium separation ($dTi-Ti$), inter ionic distance (Ri), inter-nuclear distance (ri), and polaron radius (rp)of the synthesized glasses were determined. Our results show that both the band gap and refractive index increased with TiO_2 content while Urbach energy decreased. The nuclear radiation shielding properties of these glasses were explored by utilizing Phy-X/PSD simulations. The lower value of the (MFP) sample contains higher TiO_2 content, so good glasses for γ radiation attenuation are accessible. Fast cross section neutron removal of these glasses enhanced as the concentration of TiO_2 increased. Gamma-ray shielding properties of these glasses were compared with different conventional shielding materials and commercial glasses. Therefore, the investigated glasses have potential uses in gamma shielding applications.

Keywords Borosilicate · Phy-X/PSD · Optical · Attenuation · FNRCS

1 Introduction

The specifications of materials that can serve a double function over the last century can be regarded as among the disguised targets of several researchers. Transparent glasses can be used in radiation shielding materials as a dual function. For the development of optically transparent radiation shielding materials, significant numbers of glass research labs are rising day-by-day. These materials are used in optical communication, modern optical devices, and radiation shielding materials where protection is needed from radiation [1–8].

Due to its remarkable features such as good thermal stability, hardness, chemical stability, and so on, borosilicate glasses have become the best substitute for concrete shielding, and borosilicate glasses have improved physical characteristics like transparency and refractive index. Titanium oxide, including borate, silicate, borosilicate, and phosphate glasses, one of the most significant additives in glass systems can be considered. The addition of TiO_2 has been reported to increase the glass system's network stability and mechanical characteristics. Glasses having higher amount of titanate confirmed the structural unit TiO_4, TiO_5 and TiO_6 and their physical features depend on their number of coordinates [9].

To modify the characteristics of the glass, glass modifiers are incorporated to the glass network. Alkali halides [10–12] such as LiF, and some transition metals like ZnO, and TiO_2 are included in modifiers. The melting temperature of glass and its viscosity can be affected by glass modifiers while retaining its

✉ Kh. S. Shaaban
khamies1078@yahoo.com

[1] Chemistry Department, Faculty of Science, Al-Azhar University, P.O. 71524, Assiut, Egypt

[2] Department of Physics, Faculty of Science, King Khalid University, P.O. Box 9004, Abha, Saudi Arabia

[3] Faculté des Sciences de Sfax, Département de Physique, Laboratoire des matériaux composites céramiques et polymères (LaMaCoP) Faculté des sciences de Sfax BP 805, Université de Sfax, Sfax 3000, Tunisie

[4] Laboratoire de Physique Appliquée, Groupe des Matériaux Luminescents, Université de Sfax, Faculté des Sciences de Sfax, BP 1171, 3000 Sfax, Tunisia

[5] Department of Physics, Sakarya University, Sakarya, Turkey

chemical structure, as well as affecting its optical, mechanical, thermal, and shielding ability. To generate mobile ion species Li^+, Na^+, etc., halides such as NaF, LiF, are introduced into the glass matrix. So that, halide glasses are excellent reagents for metal ions. Glasses incorporating halide ions have long been studied due to their unique physical characteristics.

The emergence of TiO_2 into the glass network improved the glass's optical, mechanical, thermal, and shielding characteristics [12, 13]. Because of the good ionic conductivity of these glasses, it is extremely possible to use them in UV optics, solid-state batteries, and radiation protection. Depending on their concentration in the glass matrix, intermediate oxides such as TiO_2 can act as either a glass modifier or former. TiO_2 improves the mechanical strength and radiation protection of the host glass matrices. These glasses possess lower photon energy and greater refractive index than other glasses. The significant development of lithium fluoride zinc titanate borosilicate glasses is very important scientifically and technologically. In this study the TiO_2 increased at expense of ZnO. With an increasing in TiO_2 content the composition changes in the glass network and increase the glass network connectivity. Due to this increase will be transform of Si– O– Zn into Si– O– Ti,and Zn– O bond strength is (73 kcal/mol) is much lower than Ti– O (73 kcal/mol) [14]. This is clearly demonstrated on the modification role of a TiO_2 in the glass system. The introduction of TiO_2 into the glass network enhanced the optical and physical properties of the glass.

It is the best study for the preparation of lithium fluoride zinc titanate borosilicate glasses and their structural, mechanical, shielding radiation, and optical properties. Thus, it is possible to find the lithium fluoride zinc titanate borosilicate glasses are suitable for use in environments exposed to radiation. The purposes of this research are to identify the attenuation proficiency of lithium fluoride zinc titanate borosilicate glasses using Phy-X/PSD [15] and XCOM software and to identify the mechanical and structure of these glasses to determine their suitability as gamma-ray shielding materials.

2 Experimental Processes and Techniques

Glass samples in Table 1 were formulated using the melt-quench method in the chemical formula $29SiO_2 – 2LiF – 59B_2O_3 – (10\text{-}x)\ ZnO – x\ TiO_2$, where $x = 0, 2, 4, 6, 8,$ *and* 10 mol %. SiO_2, LiF, H_3BO_4, ZnO and TiO_2 are the initial materials for obtaining these glasses. All the initial materials that have been acquired from Sigma-Aldrich Company. Through grinding the blend repetitively to obtain a fine powder, the starting materials were blended. First, to eliminate H_2O and other impurities, the base materials were heated to 650 °C for 1 h. The heat was increased for 45 min to 1200 °C. To reduce the internal stresses, the samples were annealed at 450 °C for 2 h and left to cool slowly to ambient temperature. The glass samples amorphous state was checked using X-ray diffraction (A Philips X-ray diffractometer PW/1710). Optical parameters were predictable by using spectrophotometer type JASCO, V-670 (Japan). In the research, Phy-X/PSD software was used to compute all radiation parameters, and these parameters are calculated by following equations: The mean free path (MFP) was predictable as $MEP = \left(\frac{1}{\mu}\right),.$ Electron density (N_{eff}) was predictable as: $N_{eff} = N\ \frac{Z_{eff}}{\sum_i F_i A_i},.$ Effective cross-section of removal (Σ_R) predicted as: $\left(\frac{\Sigma_R}{\rho}\right) = \sum_i w_i \left(\frac{\Sigma_R}{\rho}\right)_i$ and $R = \sum_i \rho_i \left(\frac{R}{\rho}\right)_i,.$

Table 1 Chemical compositions of the prepared glasses (mol, %)

Sample name	Chemical Composition				
	B_2O_3	SiO_2	LiF	ZnO	TiO_2
G 1	59	29	2	10	0
G 2	59	29	2	8	2
G 3	59	29	2	6	4
G 4	59	29	2	4	6
G 5	59	29	2	2	8
G 6	59	29	2	0	10

3 Results and Discussions

3.1 Physical Observations

As exemplified in Fig. 1, no discrete lines, no sharp peaks, were confirmed by XRD patterns and signify that the samples have a high amorphous state. The width of the halo varies through one sample to another, but no indication of the crystalline phase has been shown in all the samples.

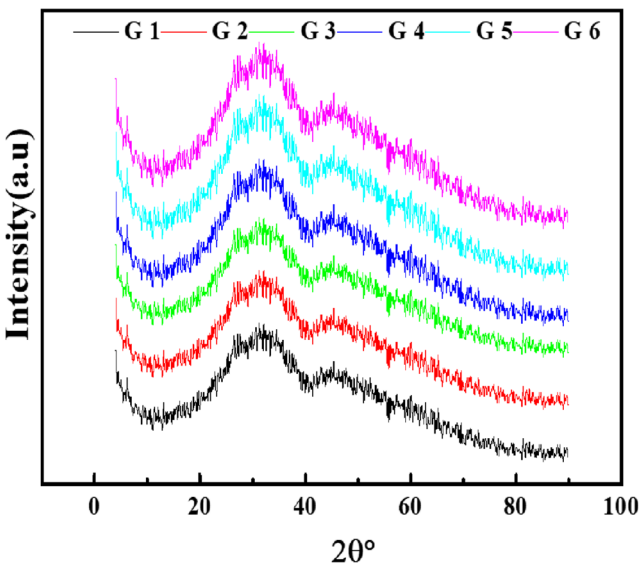

Fig. 1 XRD of the studied glasses

Titanium ion concentration computed as, $Ti^{+4} = \left(\frac{6.023\times10^{23}x\ mol\ fraction\ of\ cation\times valency\ of\ Ti}{Vm}\right)$, where V_m molar volume, titanium ion concentration increased due to the molar volume decrease. Inter-ionic distance $R_i = \left(\frac{1}{\text{Concentration of Ti}}\right)^{\frac{1}{3}}$, inter-nuclear distance (r_i) and polaron radius (r_p) computed as $rp = \frac{1}{2}\ \left(\frac{\pi}{6N}\right)^{\frac{1}{3}}$, $ri = \left(\frac{1}{N}\right)^{\frac{1}{3}}$ [16–32]. Titanium – Titanium separation ($dTi-Ti$) computed as $(\text{dTi–Ti}) = \left(\frac{V_m^B}{N}\right)^{\frac{1}{3}}$ and $V_m^B = \frac{Vm}{2(1-2Xn)}$, is the borate molar volume in 1 mol and x_n is considered as the mole fraction of B_2O_3 and N is Avogadro's number. It has been confirmed that these perceived values reduce with TiO_2 due to the molar volume decrease.

Molar refractivity (R_m), molar polarization ($\propto_m$), and loss of reflection R_L, [33–37] of the prepared glasses are computed as: $R_m = Vm\left(1-\sqrt{Eopt./20}\right)$, $\propto_m = \left(\frac{3}{4\pi N}\right)R_m$, $R_L = \left(\frac{R_m}{Vm}\right)$, where *Eopt*. Optical bandgap. The values of these parameters decreased due to the molar volume decrease. The indicator for metallization is estimated as $M = 1-\frac{R_m}{Vm}$. Because of the reduction in molar volume and (R_L), metallization is reduced. In Table 2, the above predicted results are shown.

The coordinated average number is a significant criterion for BO or NBO connection confirmation and characterized as $m = \sum n_{ci}X_i$ where cation coordination is n_{ci} and X_i *is mole fraction of the glass compoenet*. It was noticed that m increases with increase in TiO_2 content. Calculate the number of bonds per unit as $n_b = \frac{N_A}{V_m}\sum n_{ci}X_i$. It was discovered that perceived n_b through TiO_2 content increased.

The bulk module (K) and glass transition temperature ($T_{g(thero.)}$ are straight comparative to optical bandgap E_{opt} and predictable as $K_{th} = -478.93 + 200.13\ E_{opt.}$, $T_{g(thero.)} = -701.87 + 403.33\ E_{opt.}$.It suggested that these increment with TiO_2 because of an increase in bandgap energy.

Cohesive energy values are predicted as $CE(Kcal/mol) = 18.17 + 4.53 * E_{opt.}\ (e.\ V)$ or $CE(e.\ V/atom) = 0.792 + 0.198 * E_{opt.}\ (e.\ V)$. $E_{opt.}$ has a direct proportion with cohesive energy. Consequently, with the rise in the TiO_2 content, the cohesive energy value rises.

The theoretical prediction of band-gap energy $E_{opt}^{Th} = \sum Eopt\ X_i$, $E_{opt}^{Th} = 3.71*\chi$ and $E_{opt}^{Th} = 1.08*\chi^2-1.36)$, where X_i *is mole fraction of the glass compoenet* and χ is electronegativity. The theoretically bandgap rate increases with an increasing of TiO_2. The whole rising energy bandgap values is probable because of the formation of the BO.

Theoretical optical basicity $\wedge_{th}$ can be computed for glass samples $\wedge_{th} = \sum \wedge_{th}X_i$ where $\wedge$ is optical basicity of oxides and X_i fraction of each oxide. This decrease in the values of the $\wedge_{th}$ is because of the differences of $\wedge_{th}$between TiO_2 (0.97), and ZnO (1.13) [33–37].

The two-photon absorption factor TPA (β) cm / GW, expressed as $\beta = 36.67 - 8.1E_{opt}$ where E_{opt} bandgap energy. β value was observed to reduce with the increase in the content of TiO_2 because of increase in E_{opt}.

The ionic and covalent character of glasses could be estimated as the electronegativity difference. $\Delta X = \sum X_i\Delta X_i$, *where* $\Delta X_i = X_O - X_M$, $I_b = [1-e^{(-0.25)(X^2)}]$ where I_b Ionicity. With the increment in TiO_2 content and reduce in covalency I_c, it was found that (I_b) enhanced.

The glass network is influenced by the total number of mechanical constraints and computed as $N_{con} = N_{bs} + N_{bb}$ where N_{bb} is bond bending constraints and N_{bs} is bond stretching, $N_{bb} = \frac{\sum xi\ m}{2}$, $N_{bs} = \sum xi(2m-3)$. The N_{con}, N_{bs} *and* N_{bb}. With an increment in TiO_2, the overall constraints of N_{con} are expected to increase. Floppy modes considered as $M_f = 2-\frac{5m}{6}$, cross-linking density D_{CL} considered as $D_{cl} = N_{con} - 2$, $CN_{eff} = \frac{2}{5}\ N_{con} + 3$. Results are calculated increase with increasing in TiO_2 content. From the data result, it can therefore be suggested that the glass 's retained its 2D network with an increment in TiO_2.

Lone-pair electrons (L) play a major role in the formation of glass and thermal stability. It calculated as $L = V - m$

Table 2 Various physical parameters of the studied glasses

Samples	G 1	G 2	G 3	G 4	G 5	G 6
Molar Refractivity R_m (cm^3/mol)	15.52	14.745	14.15	13.36	12.7	12.22
Molar Polarizability $\propto_m$ ($A^{\circ 3}$)	6.18	5.85	5.6	5.3	5.04	4.85
Reflection loss (R_2)	0.587	0.5865	0.5862	0.586	0.585	0.5848
Metallization criterion (M)	0.413	0.4135	0.4138	0.414	0.4144	0.4147
Electron Polarizability (α°)	2.68	2.67	2.67	2.67	2.669	2.668
Ion conc. (N_i) (10^{21} ions/cm^3)	–	1.92	3.99	6.35	8.9	11.56
Inter ionic Distance Ri (A°)	–	8.179	6.41	5.49	4.91	4.5
Inter-nuclear distance, ri (Å)	–	9.474	7.436	6.385	5.71	5.24
Polaron radius, r_p (Å)	–	2.72	2.135	1.8	1.64	1.5
Ti-Ti separation($d_{Ti\text{-}Ti}$), nm	0.5	0.492	0.483	0.47	0.46	0.45

Where, V is valence electron number and m coordinated average number. The values of $L\&V$ are directly related to the TiO_2. This is because of an increase in the rigidity of the glass matrix. The increment in the L values confirmed that there is a reduction in stress energy. The increment number of coordinates could further signify the above. In Table 3, the above predicted results are shown.

3.2 Optical Investigations

Figure 2 exemplifies the absorbance (A) and transmittance (T) and reflectance (R) of glass samples. Optical absorption was quantified to understand the optical characteristics of the prepared glasses [16–32]. Then, with the same approach, we computed the required absorption coefficient for these glasses. There have been indications of decreasing the absorption coefficient as Fig. 3.

E_{opt} is observed as α. $h\nu = C(h\nu - E_{opt})^s$ where s = 2. E_{opt}values were computed and are illustrated in Fig. 4 and Table 3. The indirect optical band that was collected was identified to be 3.41 for G 1, 3.42 for G 2, 3.425 for G 3, 3.43 for G 4, 3.435 for G 5 and 3.44 for G 6. Particularly,

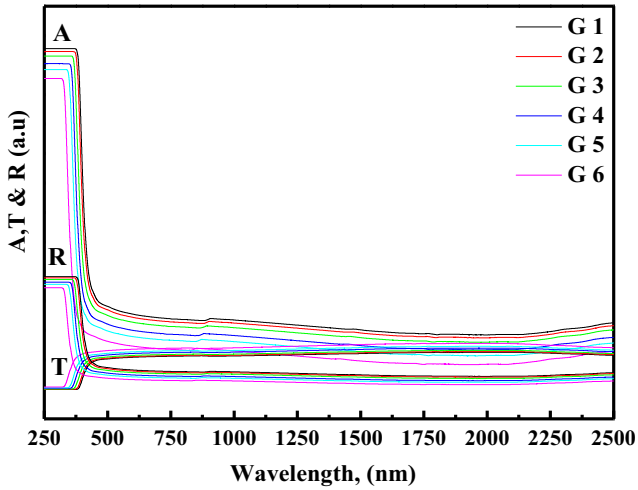

Fig. 2 Absorbance (A), Transmittance (T), and Reflectance (R) of prepared glasses a function of wavelength and with varying quantities of TiO_2

Table 3 Various physical and optical parameters of the studied glasses

Samples	G 1	G 2	G 3	G 4	G 5	G 6
Average coordination number (m)	3.74	3.78	3.82	3.86	3.9	3.94
Number of bonds per unit volume n_b (10^{29} m^{-3})	8.52	9.05	9.53	10.2	10.8	11.4
Indirect bandgap (e.V)	3.41	3.42	3.425	3.43	3.435	3.44
Number of oxygen atom	2.45	2.47	2.49	2.51	2.53	2.55
Glass transition temperature (K)	673.5	677.52	679.5	681.55	683.57	685.6
Bulk modulus (Gpa)	203.5	205.5	206.5	207.52	208.52	209.52
Electronegativity (χ)	0.9166	0.9193	0.92	0.92	0.92	0.92
Theoretically Electronegativity (χ)	1.5116	1.5138	1.516	1.5182	1.5204	1.5226
Optical basicity ($_{th}$)	1.2417	1.24035	1.24	1.239	1.23834	1.2376
Theoretically optical basicity ($_{th}$)	0.6517	0.6473	0.6429	0.6385	0.6341	0.6341
The two-photon absorption coefficient (TPA)	9.139	9.058	9.0175	8.977	8.9365	8.896
Ionicity (I_b)	0.435	0.436	0.437	0.438	0.439	0.44
Covalency (I_c)	0.565	0.564	0.563	0.562	0.561	0.56
bandgap theoretically (e.V)	8.054	8.06	8.066	8.072	8.078	8.078
Duffy bandgap theoretically (e.V)	5.6	5.616	5.62	5.63	5.64	5.65
Di-Qurato bandgap theoretically (e.V)	2.215	2.223	2.244	2.258	2.273	2.288
Cohesive Energy, CE_{ind} (Kcal/mol)	33.62	33.66	33.685	33.71	33.73	33.75
Cohesive Energy, CE_D (Kcal/mol)	1.467	1.469	1.47	1.471	1.472	1.473
Bond-stretching constraints, N_{bs}	1.87	1.89	1.91	1.93	1.95	1.97
Bond-bending constraints, N_{bb}	2.24	2.28	2.32	2.36	2.4	2.44
Total number of constraints, N_{con}	4.11	4.17	4.23	4.29	4.35	4.41
The floppy modes, M_f	1.12	1.15	1.18	1.22	1.25	1.28
The cross-linking density, D_{CL}	2.11	2.17	2.23	2.29	2.35	2.41
Effective coordination number CN_{eff}	4.644	4.668	4.692	4.716	4.74	4.764
The number of the valance electrons, V	3.15	3.19	3.23	3.27	3.31	3.31
The lone-pair electrons number, L_p	6.89	6.97	7.05	7.13	7.21	7.25
Urbach energy (Eu) (eV)	0.565	0.556	0.544	0.52	0.509	0.48

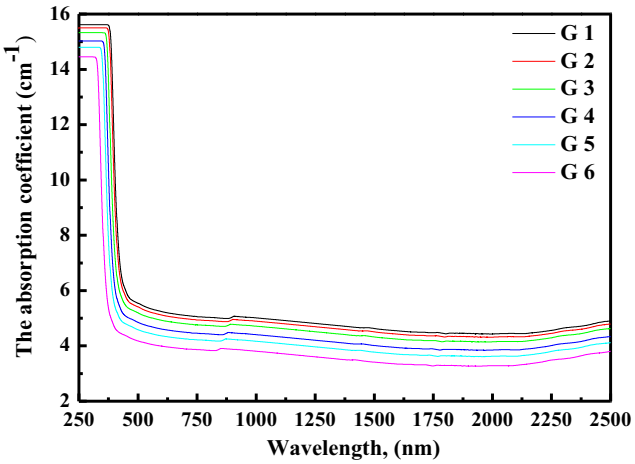

Fig. 3 The absorption coefficient (cm $^{-1}$), of prepared glasses a function of wavelength and with varying quantities of TiO_2

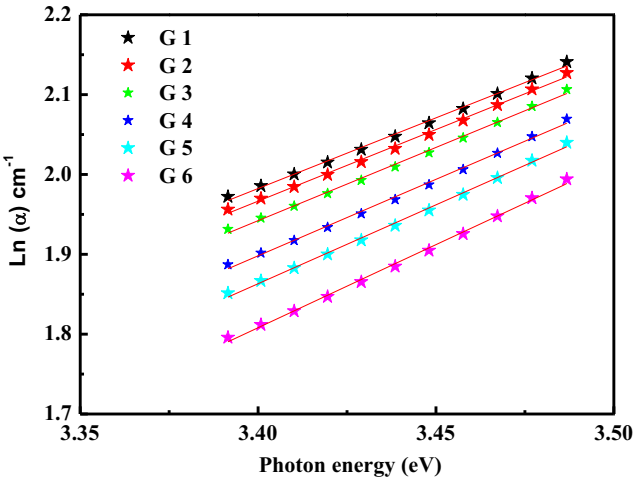

Fig. 5 Dependence of ln(α) upon the photon energy (hυ) for the prepared glasses

the optical band gap suggests the required energy to absorb light, where it requires more energy to be absorbed than in the bandgap. It has been suggested that the energy gap is increasing with the rise in TiO_2 content. The raise in the optical bandgap, confirmed that more bridging oxygen (BO) was developed. Hence, (BO) bind energized electrons more strongly than non-bridging oxygen (NBO). As the content of TiO_2 increased, this increase resulted in a change in the composition of the glass matrix and increased the interconnection. Figure 5 exemplifies the logarithm of absorption coefficient as a function of energy for determining the Urbach energy from the curve slope. In Table 3, the observable Urbach energies are computed. This reduces as the concentration of TiO_2 raised.

The refractive index of manufacturing glass (n) was already computed as: $n = \frac{(1-R)^2+k^2}{(1+R)^2+k^2}$ where $k = \alpha\lambda/4\pi$. (n) of manufacturing glasses obtainable in Fig. 6, it was observed that the refractive index of the investigated glasses are increases as density increase. There is a direct correlation between the density and refractive index, i.e., the denser the glass study, the greater the refractive index. So, the refractive index is exactly applicable to reflectance and density, and the molar volume is inversely comparable.

Molar polarization R_m, and polarizability $\propto_m$ of glasses were expected as [33–37] $R_m = \langle n^2 - 1 | n^2 + 2 \rangle Vm$, $\propto_m = (3|4\pi N)R_m$, and $\propto_0^{2-} = \frac{\left[\frac{Vm}{2.52}\left(\frac{n^2-1}{n^2+2}\right)-\sum\propto_{cat}\right]}{N_o^{2-}}$. The optical fundamentality of the samples prepared was linked to polarization; $\Lambda = 1.67\left(1-\frac{1}{\propto_0^{2-}}\right)$. Figs. 7, 8, 9 presented the molar PolarizabilityR_m, polarizabilities $\propto_m$ and optical basicity Λ respectively of the samples prepared, it was observed that the same trend of refractive index with concentrations of TiO_2 increased.

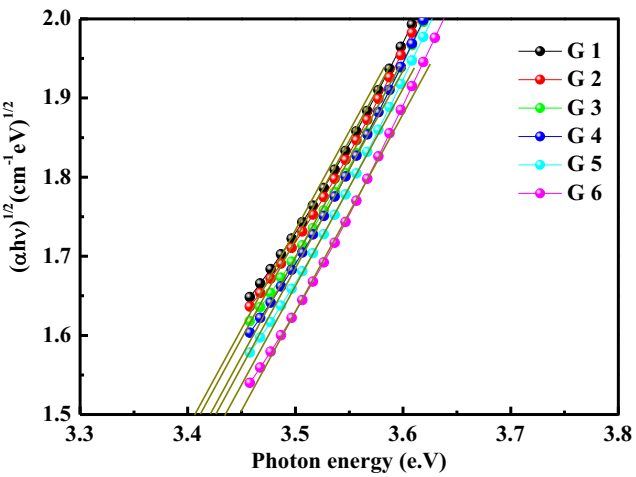

Fig. 4 Plot of $(\alpha\ h\nu)^{1/2}$ against photon energy (hν) to calculate the direct optical band gap from the intercept of the curves

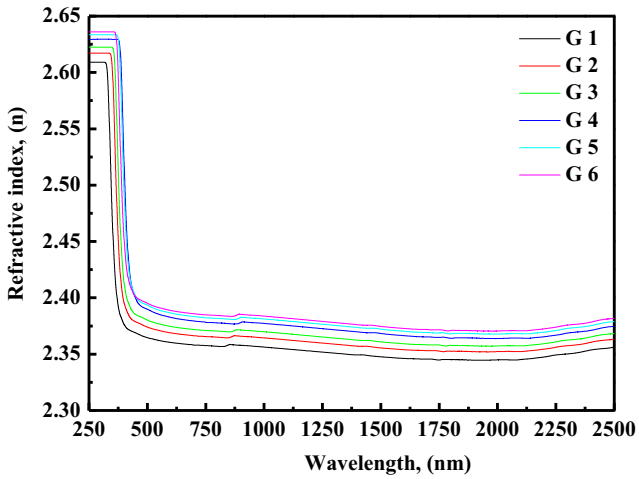

Fig. 6 Refractive index of prepared glasses a function of wavelength and with varying quantities of TiO_2

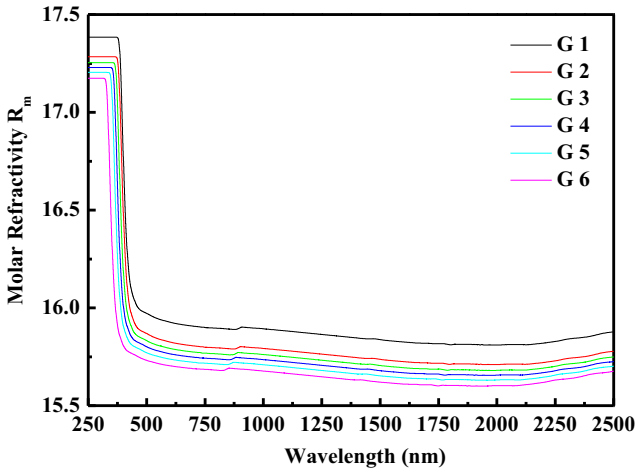

Fig. 7 Molar refractivity of prepared glasses a function of wavelength and with varying quantities of TiO_2

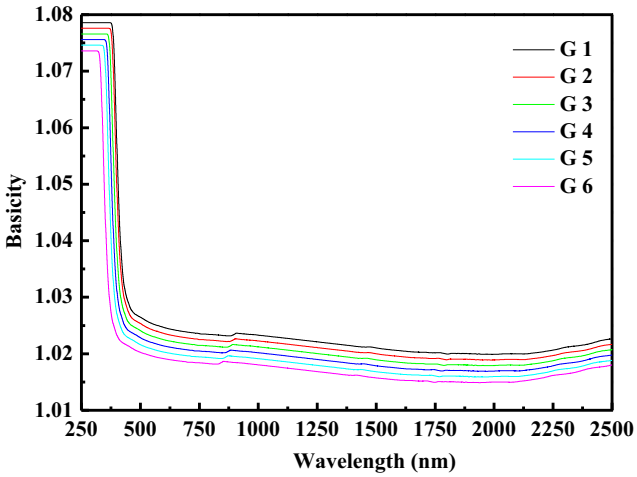

Fig. 9 Optical basicity of prepared glasses a function of wavelength and with varying quantities of TiO_2

3.3 Photon Shielding Features

In this article, the level of protection was evaluated by raising TiO_2 at the expense of ZnO with the composition $59B_2O_3 - 2LiF - 29SiO_2 - (10 - x)ZnO - xTiO_2$, $(0 \leq x \geq 10)$. In Fig. 10 the mean free path (MFP) was shown. It mentioned that the values of (MFP) are increasing as photon energy increases [38–45]. MFP is an indispensable parameter in assessing a material's gamma shielding competence, and commonly, the lower this value, the higher the shielding performance concerning sample thickness requirements. This inspiration indicated that the growth in energy makes the photon capable of transmitting samples intentionally [38–45]. The lower value of the (MFP) sample contains higher TiO_2 content, so good glasses for γ radiation attenuation are accessible. The comparison MFP of glasses with standard materials is shown in Fig. 11. These findings confirmed that glass containing a higher TiO_2 content had the greatest shielding efficiency.

To evaluate of absorbed doses and dose rates in medical dosimetry for shielding materials, assessment of effective electron density (N_{eff}) is essential. Figure 12 The (N_{eff}) values of samples against energy were illustrated. With the rise of energy, it is shown that (N_{eff}) reduces and then rises. For this reduction, the Compton scattering interaction is accountable. The increase in (N_{eff}) is attributed to the impact of creating pairs at higher energy levels with the increase in TiO_2 content. Figure 13 demonstrates the pair production of glass system as a versus photon energy. It mentioned that the pair production of these samples in increased with an increase energy.

Figure 14, 15 illustrations the ASC and ESC of glass samples against the energy of photons. It is proposed that the ASC and ESC values will reduce with the increase in energy. Because of the Compton scattering interaction, this reduction

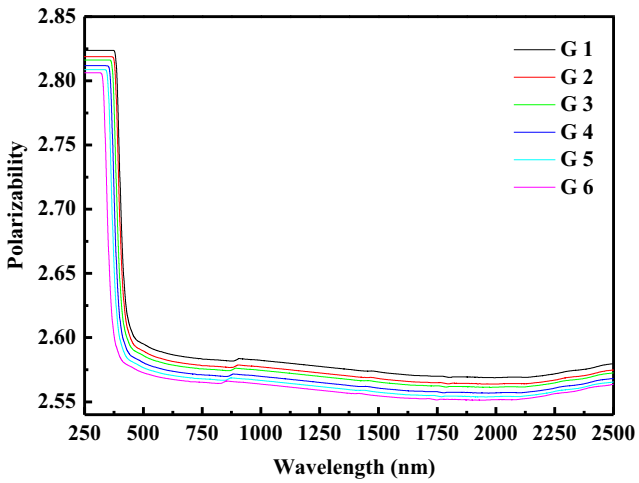

Fig. 8 Polarizability of prepared glasses a function of wavelength and with varying quantities of TiO_2

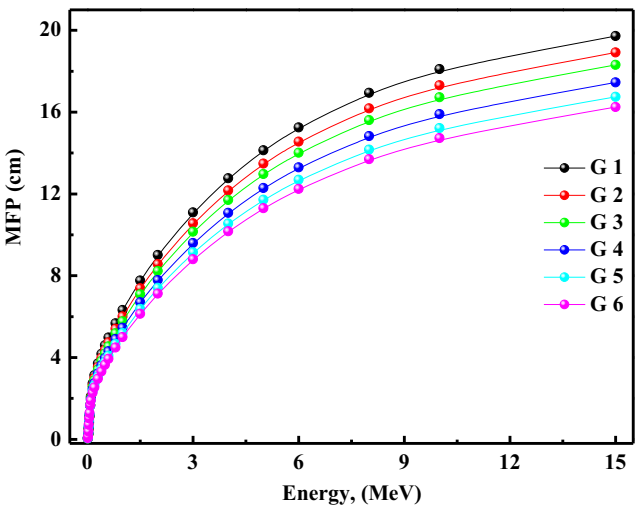

Fig. 10 The MFP for the prepared glasses as a function of photon

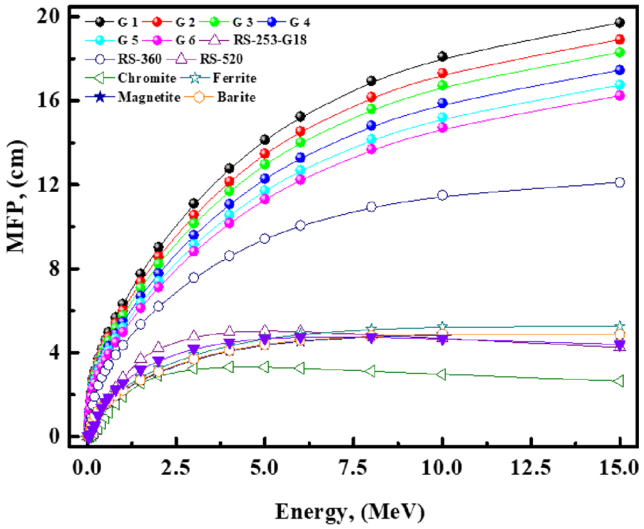

Fig. 11 The comparison MFP of glasses with standard materials

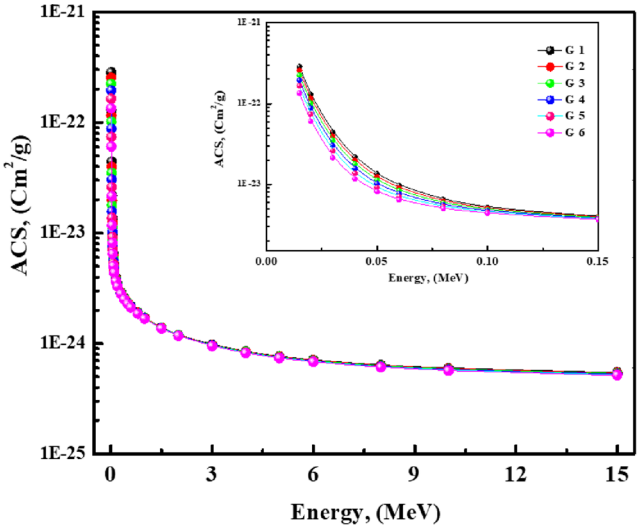

Fig. 14 The ASC for the prepared glasses as a function of photon energy

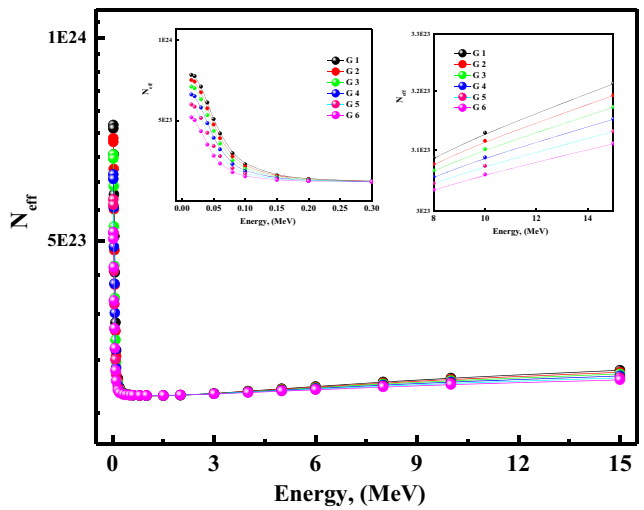

Fig. 12 The (N_{eff}) for the prepared glasses as a function of photon energy

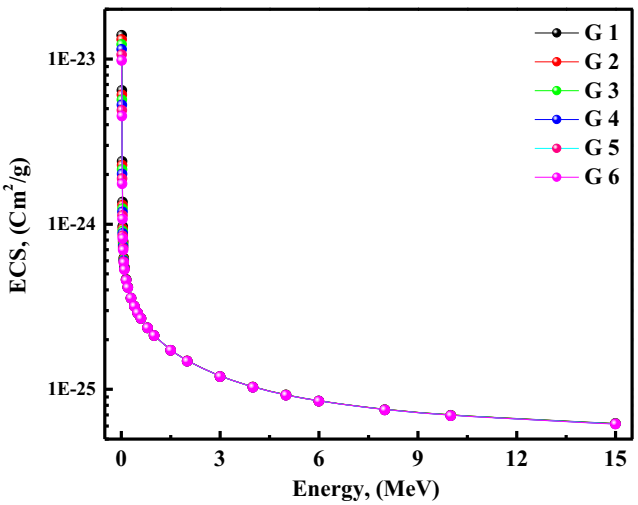

Fig. 15 The ECS for the prepared glasses as a function of photon energy

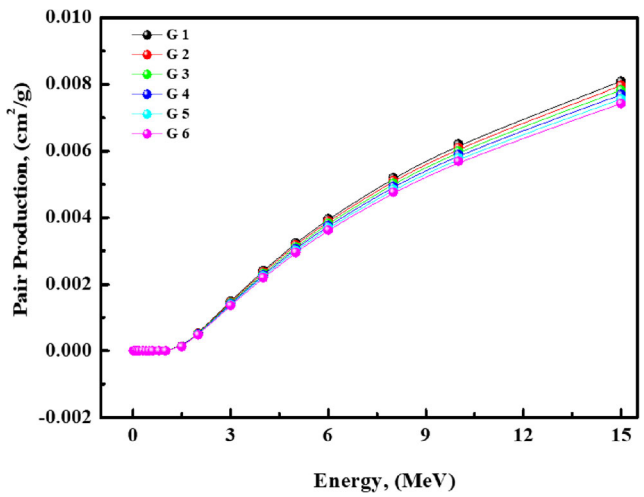

Fig. 13 The pairs production of the prepared glasses as a function of photon energy

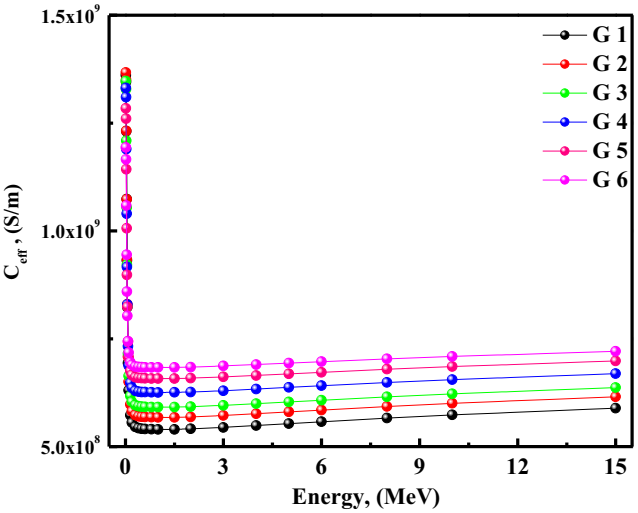

Fig. 16 The C_{eff} for the prepared glasses as a function of photon energy

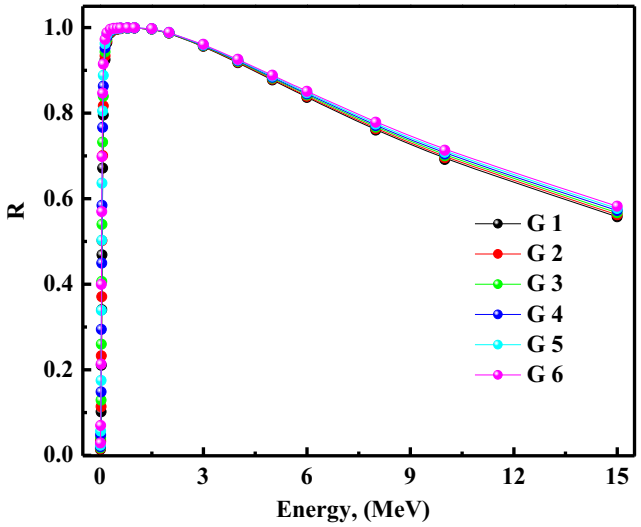

Fig. 17 Effective removal cross-through (ΣR) for the prepared glasses as a function of photon energy

occurs. Figure 16 depicted the C_{eff} against the gamma energy of these glasses. It is proposed that C_{eff} will reduce with the rise in photon energy. The increase in C_{eff} corresponded to the impact of pair-creation.

Cross-through effective removal (ΣR) of examined glasses with energy categorised in Fig. 17. It is indicated that the (ΣR) increased at lower energy. At greater energy, a reduction in the value of (ΣR) are detected. Fast cross section neutron removal (FNRCS) is obtainable in Fig. 18. It mentioned that, with TiO_2, FNRCS enhanced.

4 Conclusions

The effect of different TiO_2 concentrations on the spectroscopic and nuclear shielding properties of lithium fluoride zinc titanate borosilicate glasses with the form $59B_2O_3$-$29SiO_2$-2LiF-$(10-x)$ZnO-$xTiO_2$ $x = 0$, 2, 4, 6, 8, *and* 10 mol %. The amorphous nature of the glasses was determined by XRD measurements. The coordinated average number, Ionic concentration, bulk module (K), glass transition temperature, cohesive energy, theoretically bandgap, ionicity, mechanical constraints, floppy modes, lone-pair electrons, metallization criterion, number of bonds, and electronegativity variation with a composition also increase because of the differences in electronegativity of TiO_2 and ZnO. Molar volume, covalency, molar refractivity, molar polarizability, reflection loss, electron polarizability, inter ionic distance, inter-nuclear distance, polaron radius, and Ti-Ti separation variation with a composition also decrease because of the molar volume decrease. Our results show that both the band gap and refractive index increased with TiO_2 content while Urbach energy decreased. The nuclear radiation shielding properties of these glasses were explored by utilizing Phy-X/PSD simulations. The lower value of the (MFP) sample contains higher TiO_2 content, so good glasses for γ radiation attenuation are accessible. Fast cross section neutron removal of these glasses enhanced as the concentration of TiO_2 increased. Gamma-ray shielding properties of these glasses were compared with different conventional shielding materials and commercial glasses. Therefore, the investigated glasses have potential uses in gamma shielding applications.

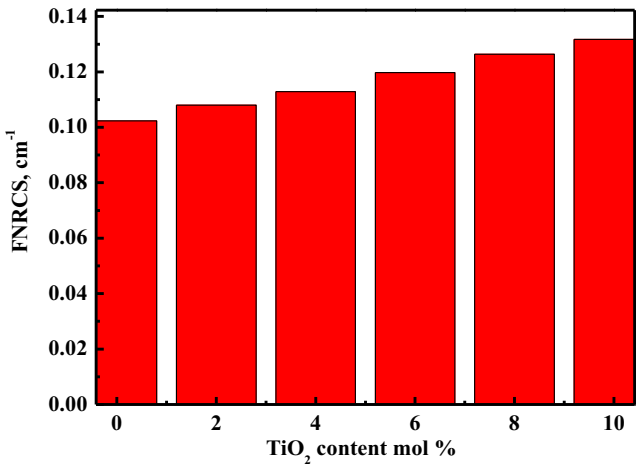

Fig. 18 FNRCS for the prepared glasses comparison with standard materials

Acknowledgments The authors extend their appreciation to the Deanship of Scientific Research at King Khalid University, Saudi Arabia for funding this work through Research Groups Program under grant number R.G.P.1/237/42.

Author Contributions **Kh. S. Shaaban**: performing XRD, UV measurements and analysis, Writing-review, writing manuscript, Methodology, Software, and writing – discussion.

Imed Boukhris, Imen Kebaili, and M.S. Al-Buriahi: These authors were listed as they reviewed this paper scientifically and linguistically and helped me in the responses to the reviewers.

Availability of Data and Material My manuscript and associated personal data will be shared with Research Square for the delivery of the author dashboard.

Declarations

The manuscript has not been published elsewhere and that it has not been submitted simultaneously for publication elsewhere.

Conflict of Interest The authors declare that they have no conflict of interest. The authors declare that they have no known competing financial interests or personal relationships that could have appeared to influence the work reported in this paper.

Consent to Participate The authors consent to participate.

Consent for Publication The authors consent for publication.

References

1. El-Damrawi G, Abdelghany AM, Hassan AK et al. (2020) Effect of BO_4 and FeO_4 structural units on conduction mechanism of Iron borosilicate glasses. Silicon. https://doi.org/10.1007/s12633-020-00694-w
2. Shaaban KS, Wahab EAA, Shaaban ER, Yousef ES, Mahmoud SA (2020) Electronic Polarizability, optical basicity, thermal, mechanical and optical investigations of ($65B_2O_3$–$30Li_2O$–$5Al_2O_3$) glasses doped with Titanate. J Elec Mater 49:2040–2049. https://doi.org/10.1007/s11664-019-07889-x
3. Shaaban KS, Abo-Naf SM, Hassouna MEM (2019) Physical and structural properties of Lithium borate glasses containing MoO_3. Silicon 11:2421–2428. https://doi.org/10.1007/s12633-016-9519-4
4. Abdel Wahab EA, Shaaban KS, Elsaman R, Yousef ES (2019) Radiation shielding, and physical properties of lead borate glass doped ZrO_2 nanoparticles. Appl Phys A Mater Sci Process 125:869. https://doi.org/10.1007/s00339-019-3166-8
5. Abd-Allah WM, Saudi HA, Shaaban KS, Farroh HA (2019) Investigation of structural and radiation shielding properties of $40B_2O_3$–30PbO–(30-x) BaO-x ZnO glass system. Appl Phys A Mater Sci Process 125:275. https://doi.org/10.1007/s00339-019-2574-0
6. Shaaban KS, Abo-naf SM, Abd Elnaeim AM, Hassouna MEM (2017) Studying effect of MoO_3 on elastic and crystallization behavior of lithium diborate glasses. Appl Phys A Mater Sci Process 123(6). https://doi.org/10.1007/s00339-017-1052-9
7. Wahab EAA, Shaaban KS (2018) Effects of SnO_2 on spectroscopic properties of borosilicate glasses before and after plasma treatment and its mechanical properties. Mater Res Express 5(2):025207. https://doi.org/10.1088/2053-1591/aaaee8
8. Shaaban KS, Yousef ES, Abdel Wahab EA, Shaaban ER, Mahmoud SA (2020) Investigation of crystallization and mechanical characteristics of glass and glass-ceramic with the compositions $x$$Fe_2O_3$-$35SiO_2$-$35B_2O_3$-$10Al_2O_3$-(20−$x$) Na_2O. J Mater Eng Perform 29:4549–4558. https://doi.org/10.1007/s11665-020-04969-6
9. Somaily HH, Shaaban KS, Makhlouf SA, Algarni H, Hegazy HH, Wahab EAA, Shaaban ER (2020) Comparative studies on Polarizability, Optical Basicity and Optical Properties of Lead Borosilicate Modified with Titania. J Inorg Organomet Polym 31:138–150. https://doi.org/10.1007/s10904-020-01650-2
10. Okasha A, Marzouk SY, Hammad AH, Abdelghany AM (2017) Optical character inquest of cobalt containing fluoroborate glass. Optik - Int J Light Electron Opt 142:125–133. https://doi.org/10.1016/j.ijleo.2017.05.088
11. Shakespeare W (2002) Halide Glass. Struct Chem Glasses:1–12. https://doi.org/10.1016/b978-008043958-7/50019-4
12. Yamane M, Kawazoe H, Inoue S, Maeda K (1985) IR transparency of the glass of $ZnCl_2$-KBr-$PbBr_2$ system. Mater Res Bull 20(8):905–911. https://doi.org/10.1016/0025-5408(85)90073-x
13. Shaaban KS, Koubisy MSI, Zahran HY, Yahia IS (2020) Spectroscopic properties, electronic Polarizability, and optical basicity of titanium–cadmium Tellurite glasses doped with different amounts of lanthanum. J Inorg Organomet Polym 30:4999–5008. https://doi.org/10.1007/s10904-020-01640-4
14. Varshneya Arun K., Fundamentals of inorganic glasses, Academic Prese Limited, (1994), p.33
15. Şakar E, Özpolat ÖF, Alım B, Sayyed MI, Kurudirek M (2020) PhyX / PSD: development of a user friendly online software for calculation of parameters relevant to radiation shielding and dosimetry. Radiat Phys Chem 166:108496. https://doi.org/10.1016/j.radphyschem.2019.108496
16. Shaaban KS, Zahran HY, Yahia IS et al (2020) Mechanical and radiation-shielding properties of B_2O_3–P_2O_5–Li_2O–MoO_3 glasses. Appl. Phys. A 126(10):804. https://doi.org/10.1007/s00339-020-03982-9
17. Saudi HA, Abd-Allah WM, Shaaban KS (2020) Investigation of gamma and neutron shielding parameters for borosilicate glasses doped europium oxide for the immobilization of radioactive waste. J Mater Sci Mater Electron 31(9):6963–6976. https://doi.org/10.1007/s10854-020-03261-6
18. El-Sharkawy RM, Shaaban KS, Elsaman R, Allam EA, El-Taher A, Mahmoud ME (2020) Investigation of mechanical and radiation shielding characteristics of novel glass systems with the composition xNiO-20ZnO-$60B_2O_3$-(20-x) CdO based on nano metal oxides. J Non-Cryst Solids 528:119754. https://doi.org/10.1016/j.jnoncrysol.2019.119754
19. El-Rehim AFA, Shaaban KS, Zahran HY et al (2020) Structural and mechanical properties of Lithium bismuth borate glasses containing molybdenum (LBBM) together with their glass–ceramics. J Inorg Organomet Polym 31:1057–1065. https://doi.org/10.1007/s10904-020-01708-1
20. El-Maaref AA, Wahab EAA, Shaaban KS, Abdelawwad M, Koubisy MSI, Börcsök J, Yousef ES (2020) Visible and mid-infrared spectral emissions and radiative rates calculations of Tm^{3+} doped BBLC glass. Spectrochimica Acta Part A: Molecular and Biomolecular Spectroscopy, 118774. doi: https://doi.org/10.1016/j.saa.2020.118774
21. Gedam RS, Ramteke DD (2012) Synthesis and characterization of Lithium borate glasses containing La_2O_3. Trans Indian Inst Metals 65:31–35. https://doi.org/10.1007/s12666-011-0107-4
22. Fayad AM, Abd-Allah WM, Moustafa FA (2018) Effect of gamma irradiation on structural and optical investigations of borosilicate glass doped yttrium oxide. Silicon 10:799–809. https://doi.org/10.1007/s12633-016-9533-6
23. Kaewjaeng S, Kothan S, Chaiphaksa W, Chanthima N, Raja Ramakrishna R, Kim HJ, Kaewkhao J (2019) High transparency La_2O_3-CaO-B_2O_3-SiO_2 glass for diagnosis x-rays shielding material application. Radiat Phys Chem 160:41–47. https://doi.org/10.1016/j.radphyschem.2019.03.018
24. Shaaban K, Abdel Wahab EA, El-Maaref AA et al (2020) Judd–Ofelt analysis and physical properties of erbium modified cadmium lithium gadolinium silicate glasses. J Mater Sci Mater Electron 31:4986–4996. https://doi.org/10.1007/s10854-020-03065-8
25. El-Maaref AA, Badr S, Shaaban KS, Wahab EAA, ElOkr MM (2019) Optical properties and radiative rates of Nd^{3+} doped zinc-sodium phosphate glasses. J Rare Earths 37(3):253–259. https://doi.org/10.1016/j.jre.2018.06.006
26. Shaaban KS, Wahab EAA, Shaaban ER, Yousef ES, Mahmoud SA (2020) Electronic polarizability, optical basicity and mechanical properties of aluminum lead phosphate glasses. Opt Quant Electron 52:125. https://doi.org/10.1007/s11082-020-2191-3
27. Shaaban KS, Yousef ES (2020) Optical properties of Bi_2O_3 doped boro tellurite glasses and glass ceramics. Optik – Int J Light Electron Opt 203:163976. https://doi.org/10.1016/j.ijleo.2019.163976
28. El-Rehim AA, Zahran H, Yahia I et al. (2020) Radiation, crystallization, and physical properties of cadmium borate glasses. Silicon https://doi.org/10.1007/s12633-020-00798-3
29. Abdel Wahab EA, El-Maaref AA, Shaaban Kh.S, Börcsök J, Abdelawwad M (2020) Lithium cadmium phosphate glasses doped Sm^{3+} as a host material for near-IR laser applications, optical Materials,110638, https://doi.org/10.1016/j.optmat.2020.110638
30. Abdel Wahab EA, Koubisy MSI, Sayyed MI, Mahmoud KA, Zatsepin AF, Makhlouf SA, Shaaban KS (2020) Novel borosilicate glass system: $Na_2B_4O_7$-SiO2-MnO_2 synthesis, average electronics polarizability, optical basicity, and gamma-ray shielding features. J Non-Cryst Solids 553:120509. https://doi.org/10.1016/j.jnoncrysol.2020.120509

31. El-Rehim AFA, Zahran HY, Yahia IS et al. (2020) Physical, radiation shielding and crystallization properties of Na_2O-Bi_2O_3-MoO_3-B_2O_3- SiO_2-Fe_2O_3 glasses. Silicon https://doi.org/10.1007/s12633-020-00827-1
32. Abdel Wahab EA, Shaaban KS, Yousef ES (2020) Enhancement of optical and mechanical properties of sodium silicate glasses using zirconia. Opt Quant Electron 52:458. https://doi.org/10.1007/s11082-020-02575-3
33. Dimitrov V, Sakka S (1996) Electronic oxide polarizability and optical basicity of simple oxides. I. J Appl Phys 79(3):1736. https://doi.org/10.1063/1.360962
34. Dimitrov V, Komatsu T (2002) Classification of simple oxides: a Polarizability approach. J Solid State Chem 163(1):100–112. https://doi.org/10.1006/jssc.2001.9378
35. Zhao X, Wang X, Lin H, Wang Z (2007) Electronic polarizability and optical basicity of lanthanide oxides. Phys B Condens Matter 392(1–2):132–136. https://doi.org/10.1016/j.physb.2006.11.015
36. Duffy, J. A. (1989). A common optical basicity scale for oxide and fluoride glasses. J Non-Cryst Solids, 109(1), 35–39, https://doi.org/10.1016/0022-3093(89)90438-9
37. Duffy JA, Ingram MD (1992) Comments on the application of optical basicity to glass. J Non-Cryst Solids 144:76–80. https://doi.org/10.1016/s0022-3093(05)80385-0
38. AlBuriahi MS, Hegazy HH, Alresheedi F, Olarinoye IO, Algarni H, Tekin HO, Saudi HA (2020) Effect of CdO addition on photon, electron, and neutron attenuation properties of boro-tellurite glasses. Ceramics International https://doi.org/10.1016/j.ceramint.2020.10.168
39. Stalin S, Gaikwad DK, Al-Buriahi MS, Srinivasu C, Ahmed SA, Tekin HO, Rahman S (2020) Influence of Bi_2O_3/WO_3 substitution on the optical, mechanical, chemical durability and gamma ray shielding properties of lithium-borate glasses. Ceram Int 47:5286–5299. https://doi.org/10.1016/j.ceramint.2020.10.109
40. Al-Buriahi MS, Somaily HH, Alalawi A et al (2020) Polarizability, optical basicity, and photon attenuation properties of Ag_2O–MoO_3–V_2O_5–TeO_2 glasses: the role of silver oxide. J Inorg Organomet Polym 31:1047–1056. https://doi.org/10.1007/s10904-020-01750-z
41. Al-Buriahi MS, Alajerami YSM, Abouhaswa AS, Alalawi A, Nutaro T, Tonguc B (2020) Effect of chromium oxide on the physical, optical, and radiation shielding properties of lead sodium borate glasses. J Non-Cryst Solids 544:120171. https://doi.org/10.1016/j.jnoncrysol.2020.120171
42. Abouhaswa AS, Mhareb MHA, Alalawi A, Al-Buriahi MS (2020) Physical, structural, optical, and radiation shielding properties of B_2O_3-$20Bi_2O_3$-$20Na_2O_2$-Sb_2O_3 glasses: role of Sb_2O_3. J Non-Cryst Solids 543:120130. https://doi.org/10.1016/j.jnoncrysol.2020.120130
43. Naseer KA, Marimuthu K, Al-Buriahi MS, Alalawi A, Tekin HO (2020) Influence of Bi_2O_3 concentration on barium-telluro-borate glasses: physical, structural, and radiation-shielding properties. Ceram Int 47(1):329–340. https://doi.org/10.1016/j.ceramint.2020.08.138
44. Abouhaswa AS, Al-Buriahi MS, Chalermpon M et al (2020) Influence of ZrO_2 on gamma shielding properties of lead borate glasses. Appl Phys A Mater Sci Process 126:78. https://doi.org/10.1007/s00339-019-3264-7
45. Gokhan K, El Agawany FI, Ilik BO, Mahmoud KA, Ilik E, Rammah YS (2021) Ta_2O_5 reinforced Bi_2O_3–TeO_2–ZnO glasses: Fabrication, physical, structural characterization, and radiation shielding efficacy. Opt Mater 112:110757. https://doi.org/10.1016/j.optmat.2020.110757